

Mapping stress and structurally controlled crustal shear velocity anisotropy in California

Naomi L. Boness* }
Mark D. Zoback } Department of Geophysics, Stanford University, Stanford, California 94305, USA

ABSTRACT

We present shear velocity anisotropy data from crustal earthquakes in California and demonstrate that it is often possible to discriminate structural anisotropy (polarization of the shear waves along the fabric of major active faults) from stress-induced anisotropy (polarization parallel to the maximum horizontal compressive stress). Stress directions from seismic stations located near (but not on) the San Andreas fault indicate that the maximum horizontal compressive stress is at a high angle to the strike of the fault. In contrast, seismic stations located directly on one of the major faults indicate that shear deformation has significantly altered the elastic properties of the crust, inducing shear-wave polarizations parallel to the fault plane.

Keywords: crustal stress, seismic anisotropy, San Andreas fault.

INTRODUCTION

It has been known for the past 25 yr that carefully used earthquake, well-bore, and geologic data can be used to map the direction and relative magnitude of in situ horizontal principal stresses in the Earth's crust (Zoback and Zoback, 1980, 1991; Zoback, 1992), and a global database of more than 10,000 crustal stress indicators, the *World Stress Map*, is now available (Zoback et al., 1989; Reinecker et al., 2005).

In this paper we present shear velocity anisotropy data from local earthquake sources as an independent tool to analyze the state of stress close to active faults on a regional scale and in geographic regions where other types of stress measurements are lacking. We use data from the Southern California Seismic Network and Northern California Seismic Network, with an emphasis on Southern California. Western California is a good place to demonstrate this method because there are many independent stress measurements, the tectonic structures are well documented, and the direction of S_{Hmax} is, in general, at a high angle to the faults, allowing us to differentiate between the two mechanisms (e.g., Zinke and Zoback, 2000).

Numerous examples of seismic anisotropy in the upper crust have been documented in the literature over the past 25 yr since it was first observed using microearthquakes (Crampin et al., 1980). The mechanisms that cause shear waves (S-waves) to split into a fast and slow component include dilatancy of microcracks due to stress (Crampin, 1991), preferential closure of macroscopic fractures in an anisotropic stress field (Boness and Zoback,

2004), aligned macroscopic fractures associated with regional tectonics (Mueller, 1991), sedimentary bedding planes (Alford, 1986), and the alignment of minerals or grains (Sayers, 1994). These mechanisms can be divided into two major categories: stress-induced and structural anisotropy (Fig. 1). Stress-induced shear anisotropy is the result of S_{Hmax} causing microcracks to open and/or preexisting macroscopic fractures to close, generating a fast direction parallel to S_{Hmax} . Stress-induced anisotropy is observed in the upper crust and the effect decreases with depth as the confining pressure increases, closing fractures in all orientations. Borehole measurements indicate that anisotropy is largest in the near surface, with values of $\sim 10\%$ (e.g., Aster and Shearer, 1991; Boness and Zoback, 2004; Liu et al., 2004), and decreases with depth. However, evidence suggests anisotropy is still $>3\%$ in the granitic rocks in California at a depth of 3 km (Boness and Zoback, 2005). Structural anisotropy occurs when macroscopic features such as fault-zone fabric, sedimentary bedding planes, or aligned minerals and/or grains polarize the S-waves with a fast direction in the plane of the feature. With knowledge of the structural elements in a region, including major faults, it is possible to determine whether anisotropy is caused by stress, structure, or a combination of both mechanisms (Zinke and Zoback, 2000). In this paper we focus on the fast polarizations of the S-waves, because they are mostly dependent on the last anisotropic medium the wave passes through (e.g., Crampin, 1991) and more robust than the delay time.

METHODOLOGY

We have devised a quality control procedure to measure S-wave splitting using micro-

earthquakes recorded on three-component seismic stations; the procedure minimizes the scatter in the data and, with careful consideration of ray paths and local geology, allows interpretation of the observed anisotropy as stress induced or structural. For each station, we search the earthquake catalog for events that are above 20 km depth and located within a cone under the station up to a maximum incidence angle of 40° within the S-wave window (Nuttli, 1961; Booth and Crampin, 1985). We filter each event with a low limit of 1 Hz and a high limit between 10 and 25 Hz (chosen to be 5 Hz above the dominant S-wave frequency) to remove high-frequency noise without degrading the waveforms. We only use data with a signal-to-noise ratio $>3:1$ (amplitude of initial S-waves relative to pre-S-wave coda) and visually inspect each seismogram and the corresponding particle motion to establish if the S-wave arrivals are impulsive enough to be picked with confidence. We use the two horizontal components to determine the anisotropy between the S-waves because we expect vertically propagating waves within the S-wave window.

We measure the S-wave splitting of each event that satisfies our quality criteria using a technique that combines covariance matrix decomposition (Silver and Chan, 1991) with cross-correlation (Bowman and Ando, 1987). The covariance matrix of the horizontal S-wave particle motion is rotated over azimuths of -90° to $+90^\circ$ in increments of 1° and over delay times of 0–50 ms in increments of the sampling frequency. The fast direction and delay time that best linearize the particle motion are determined by minimizing the second ei-

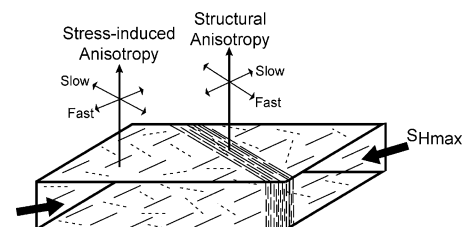


Figure 1. Schematic illustrating stress-induced anisotropy in crust adjacent to fault zone, where vertically propagating shear waves are polarized with fast direction parallel to S_{Hmax} due to preferential closure of fractures (dashed lines), and structural anisotropy of shear waves inside fault zone with fast direction parallel to fault fabric.

*Present address: Chevron, 6001 Bollinger Canyon Road, San Ramon, California 94583.

genvalue, and we compute the degree of rectilinearity (Jurkevics, 1988) from the ratio of the two nonzero eigenvalues. We only include measurements with a degree of linearity >0.8 (1 being perfectly linear). We use the maximum cross-correlation coefficient of the rotated waveforms to confirm that the seismograms have been rotated into the fast and slow polarization directions and discard any measurement with a cross-correlation coefficient <0.8 .

After the fast shear polarizations have been determined for all earthquakes at a given station, we compute the mean orientation of the fast S-waves using Fisher statistics (Fisher et al., 1987). If the azimuthal standard deviation is $<20^\circ$, we believe that the fast direction is well constrained and probably contains valuable information about either stress or structure. In contrast, standard deviations $>20^\circ$ probably indicate that a mix of mechanisms (e.g., Peng and Ben-Zion, 2004), scattering (e.g., Aster et al., 1990), or complicated local geology (e.g., Aster and Shearer, 1992) is causing the anisotropy.

RESULTS

We apply this method to data from 86 three-component stations and achieve a well-defined mean fast direction with a standard deviation of $<20^\circ$ at 62 stations (Fig. 2). The 10 stations shown in red exhibit a mean fast direction that is within 20° of the local San Andreas fault (SAF) strike (and other nearby major subparallel faults). The red rose diagrams in Figure 2 are the individual S-wave splitting measurements used to compute the mean at each of those stations (see GSA Data Repository Table DR1¹). The numbers associated with each rose diagram indicate the number of good measurements that complied with our quality control criteria out of the total number of earthquakes analyzed. Similarly, the blue stations and rose diagrams indicate stations with mean fast directions that are at an angle $>20^\circ$ to the SAF.

Nearly all of the stations exhibiting a mean fast direction subparallel to the structural fabric are located on the SAF. Four other stations with fault-parallel fast directions are located on the Calaveras fault, on the San Gabriel fault, in the Brawley seismic zone at the southern end of the SAF, and just south of the Brawley seismic zone near El Centro. Stations located in the adjacent crust tend to exhibit a fast direction at a high angle to the structure. The fast directions at these stations are con-

¹GSA Data Repository item 2006180, Table DR1, S-wave splitting measurements and examples of data analysis, is available online at www.geosociety.org/pubs/ft2006.htm, or on request from editing@geosociety.org or Documents Secretary, GSA, P.O. Box 9140, Boulder, CO 80301-9140, USA.

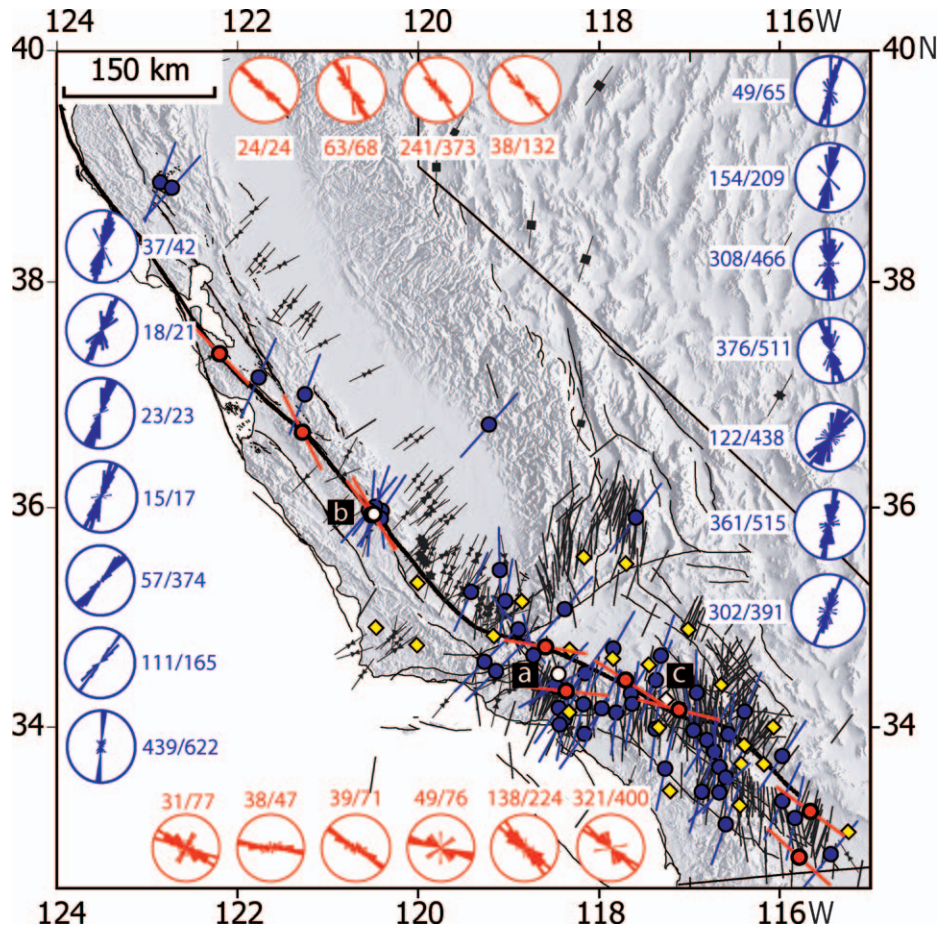


Figure 2. Map of California showing mean fast shear polarizations at stations with standard deviation $<20^\circ$. Red stations exhibit fast polarization that is subparallel to San Andreas fault and are typically located along main fault trace. Corresponding red rose diagrams show measurements of fast polarization observed at each of these stations with adjacent numbers indicating number of good quality measurements out of total number of earthquakes analyzed. Blue stations exhibit fast shear polarizations parallel to direction of S_{Hmax} (in black) determined from focal mechanism inversions (sticks) and borehole breakouts (bowties). Stations where fast azimuth standard deviation is $>20^\circ$ (yellow diamonds) indicate mix of mechanisms or scattering. Data for three white stations showing (a) stress, (b) structural, and (c) mixed anisotropy are displayed in Figure 3.

sistent with the direction of S_{Hmax} obtained from focal mechanism inversions and well-bore breakouts (data shown are from Townend and Zoback, 2004). There are a few stations located on major faults like the San Jacinto fault with fast shear polarizations that are subparallel to the stress rather than the fault fabric. There are 24 stations where the standard deviation of the fast azimuth is $>20^\circ$ (yellow diamonds in Fig. 2).

We present the earthquake data and individual S-wave splitting measurements for three stations (shown as the white stations in Fig. 2) as examples of stress-induced, structural, and mixed anisotropy observations (Fig. 3). For a typical station that shows stress-induced anisotropy (Fig. 3A), there is fairly good azimuthal coverage. For this particular station, the majority of earthquakes are located ~ 8 km to the northeast of the station at a depth of ~ 15 km. For a station located on the SAF just

northwest of Parkfield that shows structural anisotropy (Fig. 3B), the earthquakes are almost directly beneath the station and most are relatively shallow (5–8 km). One station that shows the mixed effects of structural and stress-induced anisotropy (Fig. 3C) is located ~ 8 km northeast of the SAF near San Bernardino, California.

DISCUSSION

In general, the fast directions we compute here are consistent with the results of smaller-scale anisotropy investigations in California (e.g., Aster et al., 1990; Liu et al., 1993; Lou et al., 1997; Zhang and Schwartz, 1994). However, we have analyzed a much larger number of earthquakes at each station than is typical for S-wave splitting studies (more than 100 earthquakes analyzed at 30 stations), and the scatter in the results is significantly less in this study because of our stringent quality cri-

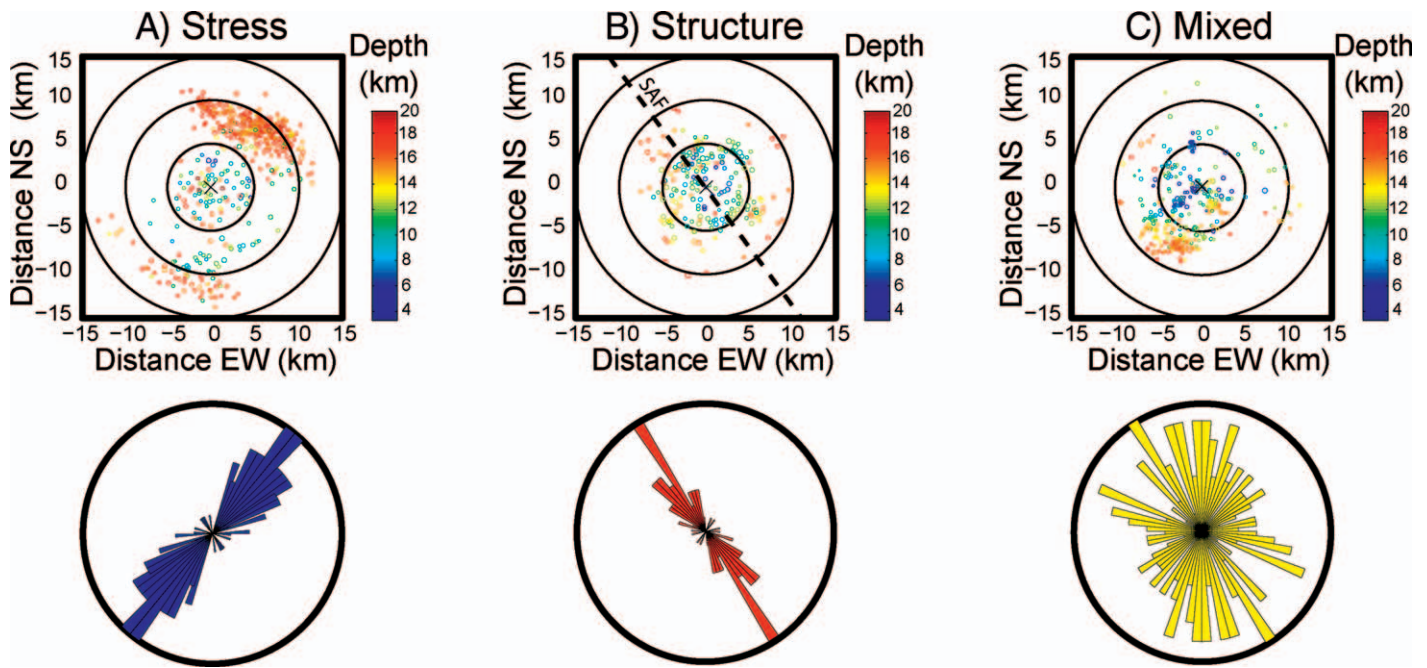


Figure 3. Example of earthquake distributions (top row) and rose diagrams showing fast polarization measurements (bottom row) for three white stations on Figure 2. **A:** Station exhibiting stress-induced anisotropy located on granite 25 km away from fault zone. **B:** Structural anisotropy is observed at station located on San Andreas fault. **C:** Mix of polarizations seen at station that is fairly close to fault and on boundary between granite and Precambrian rocks.

teria. The fault-parallel fast shear polarization at stations located on major faults (Fig. 2) implies that the physical properties of the fault zone are intrinsically different from those of the adjacent crust. The anisotropy may be caused by aligned macroscopic fractures or lithologic properties such as the presence of highly anisotropic fault gouge (e.g., Johnston and Christensen, 1995). Typically, anisotropy in the crust is $\sim 2\%$ – 4% (e.g., Li et al., 1994), the range we observe at most of the stations away from the faults, whereas the stations with a fault-parallel fast direction exhibit anisotropy of $\sim 8\%$ – 15% . Assuming an average shear velocity of 3 km/s (Brocher, 2005) with dominant shear frequencies of 5–20 Hz and vertical propagation up through the fault zone, the polarization of S-waves observed in this study implies that the fault-zone fabric must extend at least 150–600 m laterally. This is consistent with the lateral extent of the damage zone observed in the exhumed Punchbowl fault (Chester et al., 2005) and the low-velocity zone of the SAF observed using fault-zone-guided waves (e.g., Ben-Zion and Malin, 1991; Li et al., 1990, 2004) and inferred from waveform modeling (Leary and Ben-Zion, 1992).

Observations of the direction of S_{Hmax} near the SAF from focal mechanism inversions and well-bore data generally indicate that S_{Hmax} is at a high angle to the strike of the fault (Zoback et al., 1987; Mount and Suppe, 1987), implying that it slips at low shear stress. Independent studies using focal mechanism in-

versions (Hardebeck and Hauksson, 1999; Townend and Zoback, 2004; Hardebeck and Michael, 2004) all indicate that S_{Hmax} is at a high angle (60° – 90°) to the strike of the fault at distances $> \sim 15$ km. Closer to the fault (~ 10 – 15 km) the state of stress is more uncertain; different techniques used to group earthquakes for focal mechanism inversion yield stress orientations that range between 50° and 80° (e.g., Townend and Zoback, 2001; Hardebeck and Michael, 2004). Several studies indicate the possibility of a very localized rotation of S_{Hmax} to an angle of $\sim 45^\circ$ to the strike of the fault within 1–3 km of the fault plane (Hardebeck and Michael, 2004; Provost and Houston, 2001, 2003).

Figure 2 shows that the mean fast directions in the crust outside of known faults correlate very well with the direction of S_{Hmax} determined from borehole breakouts and focal mechanism inversions, and indicate that S_{Hmax} is at an angle of 60° – 90° to the strike of the fault, consistent with the hypothesis of a weak fault. While many stations exhibiting stress-induced anisotropy are near previous measurements of S_{Hmax} , we have also observed stress-induced anisotropy in locations where there were no stress data because of inadequate focal mechanism data. This illustrates the application of this method for stress mapping globally in regions with too few earthquakes for a reliable focal mechanism inversion.

At this scale, the observations of S-wave splitting at Parkfield appear to indicate both structural and stress-induced anisotropy in the

same location (in addition to two stations indicating a mix of mechanisms). However, if one examines this region in more detail it becomes apparent that the two stations with structural anisotropy are located immediately on the SAF and in the southwest fracture zone, whereas the stations exhibiting fast polarizations subparallel to the stress field are in the crust adjacent to the fault zone, ~ 5 km from the fault.

CONCLUSIONS

We show that careful use of shear velocity anisotropy data from local earthquakes is a good tool for analyzing the direction of S_{Hmax} at a regional scale. The benefits of using S-wave anisotropy are that data from any three-component seismic station can be utilized and stations close to major faults can reveal information about the stress field that are not observable with other techniques, as well as the anomalous physical properties associated with major fault zones. The application of this method to California indicates that the major active faults have intrinsically different physical properties to the adjacent crust over a lateral extent of at least 150–600 m, and that the SAF is mechanically weak, with the compressive stress at a high angle to the fault plane.

ACKNOWLEDGMENTS

We are grateful to two anonymous reviewers whose comments helped improve this manuscript. This work was supported by National Science Foundation grant EAR-0323938-001 and the Stanford Rock Physics and Borehole Project.

REFERENCES CITED

Alford, R.M., 1986, Shear data in the presence of azimuthal anisotropy: Annual International Meeting of the Society of Exploration Geophysicists Expanded Abstracts, v. 56, p. 476-479.

Aster, R.C., and Shearer, P.M., 1991, High frequency borehole seismograms recorded at the San Jacinto fault zone, Southern California, Part 1. Polarizations: Seismological Society of America Bulletin, v. 81, p. 1057-1080.

Aster, R.C., and Shearer, P.M., 1992, Initial shear wave particle motions and stress constraints at the Anza Seismic Network: Geophysical Journal International, v. 108, p. 740-748.

Aster, R.C., Shearer, P.M., and Berger, J., 1990, Quantitative measurements of shear wave polarizations at the Anza Seismic Network, Southern California: Implications for shear wave splitting and earthquake prediction: Journal of Geophysical Research, v. 95, p. 12,449-12,473.

Ben-Zion, Y., and Malin, P.E., 1991, San Andreas fault zone head waves near Parkfield, California: Science, v. 251, p. 1592-1594.

Boness, N.L., and Zoback, M.D., 2004, Stress-induced seismic velocity anisotropy and physical properties in the SAFOD Pilot Hole in Parkfield, CA: Geophysical Research Letters, v. 31, doi: 10.1029/2003GL019020.

Boness, N.L., and Zoback, M.D., 2005, Shear velocity anisotropy in and near the San Andreas fault: Implications for mapping stress orientations: Eos (Transactions, American Geophysical Union), fall meeting supplement, abs. T23E-03, v. 86, p. 52.

Booth, D.C., and Crampin, S., 1985, Shear-wave polarizations on a curved wavefront at an isotropic free-surface: Royal Astronomical Society Geophysical Journal, v. 83, p. 31-45.

Bowman, J.R., and Ando, M., 1987, Shear wave splitting in the upper-mantle wedge above the Tonga subduction zone: Royal Astronomical Society Geophysical Journal, v. 88, p. 25-41.

Brocher, T.M., 2005, Empirical relations between elastic wavespeeds and density in the Earth's crust: Seismological Society of America Bulletin, v. 95, p. 2081-2092, doi: 10.1785/0120050077.

Chester, J., Chester, F.M., and Kronenberg, A.K., 2005, Fracture energy of the Punchbowl fault, San Andreas system: Nature, v. 437, p. 133-136, doi: 10.1038/nature03942.

Crampin, S., 1991, Wave propagation through fluid-filled inclusions of various shapes: Interpretation of extensive dilatancy anisotropy: Geophysical Journal International, v. 107, p. 611-623.

Crampin, S., Evans, R., Ucer, B., Doyle, M., Davis, P.J., Yegorkina, G.V., and Miller, A., 1980, Observations of dilatancy-induced polarization anomalies and earthquake prediction: Nature, v. 286, p. 874-877, doi: 10.1038/286874a0.

Fisher, N.I., Lewis, T., and Embleton, B.J.J., 1987, Statistical analysis of spherical data: Cambridge, Cambridge University Press, 329 p.

Hardebeck, J.L., and Hauksson, E., 1999, Role of fluids in faulting inferred from stress field signatures: Science, v. 285, p. 236, doi: 10.1126/science.285.5425.236.

Hardebeck, J.L., and Michael, A.J., 2004, Stress orientations at intermediate angles to the San Andreas fault, California: Journal of Geophysical Research, v. 109, p. B11303, doi: 10.1029/2004JB003239.

Johnston, J.E., and Christensen, N.I., 1995, Seismic anisotropy of shales: Journal of Geophysical Research, v. 100, p. 5991-6003, doi: 10.1029/95JB00031.

Jurkevics, A., 1988, Polarization analysis of three-component array data: Seismological Society of America Bulletin, v. 78, p. 1725-1743.

Leary, P., and Ben-Zion, Y., 1992, A 200 m wide fault zone low velocity layer on the San Andreas fault at Parkfield: Results from analytic waveform fits to trapped wave groups: Seismological Research Letters, v. 63, p. 62.

Li, Y.-G., Leary, P.C., Aki, K., and Malin, P.E., 1990, Seismic trapped modes in the Oroville and San Andreas fault zones: Science, v. 249, p. 763-765.

Li, Y.-G., Henyey, T.L., and Teng, T.-L., 1994, Shear-wave splitting observations in the northern Los Angeles basin: Seismological Society of America Bulletin, v. 84, p. 307-323.

Li, Y.-G., Vidale, J.E., and Cochran, E.S., 2004, Low-velocity damaged structure of the San Andreas fault at Parkfield from fault zone trapped waves: Geophysical Research Letters, v. 31, p. L12S06.

Liu, Y., Booth, D., Crampin, S., Evans, R., and Leary, P., 1993, Shear-wave polarization and possible temporal variations in shear-wave splitting at Parkfield: Canadian Journal of Exploration Geophysics, v. 29, p. 380-390.

Liu, Y., Teng, T.-L., and Ben-Zion, Y., 2004, Systematic analysis of shear-wave splitting in the aftershock zone of the 1999 Chi-Chi, Taiwan, earthquake: Shallow crustal anisotropy and lack of precursory variations: Seismological Society of America Bulletin, v. 94, p. 2330-2347, doi: 10.1785/0120030139.

Lou, M., Shalev, E., and Malin, P., 1997, Shear wave splitting and fracture alignments at the Northwest Geysers, California: Geophysical Research Letters, v. 24, p. 1895-1898, doi: 10.1029/97GL01845.

Mount, V.S., and Suppe, J., 1987, State of stress near the San Andreas fault: Implications for wrench tectonics: Geology, v. 15, p. 1143-1146, doi: 10.1130/0091-7613(1987)15<1143:SOSNTS>2.0.CO;2.

Mueller, M.C., 1991, Prediction of lateral variability in fracture intensity using multicomponent shear-wave seismic as a precursor to horizontal drilling: Geophysical Journal International, v. 107, p. 409-415.

Nuttli, O., 1961, The effect of the Earth's surface on the S wave particle motion: Seismological Society of America Bulletin, v. 44, p. 237-246.

Peng, Z., and Ben-Zion, Y., 2004, Systematic analysis of crustal anisotropy along the Karadere-Düzce branch of the north Anatolian fault: Geophysical Journal International, v. 159, p. 253-274, doi: 10.1111/j.1365-246X.2004.02379.x.

Provost, A.-S., and Houston, H., 2001, Orientation of the stress field surrounding the creeping section of the San Andreas fault: Evidence for a narrow mechanically weak fault zone: Journal of Geophysical Research, v. 106, p. 11,373-11,386, doi: 10.1029/2001JB900007.

Provost, A.-S., and Houston, H., 2003, Stress orientations in northern and central California: Evidence for the evolution of frictional strength along the San Andreas plate boundary system: Journal of Geophysical Research, v. 108, p. 2175, doi: 10.1029/2001JB001123.

Reinecker, J., Heidbach, O., Tingay, M., Sperner, B., and Müller, B., 2005, Release 2005 of the World Stress Map: www.world-stress-map.org (November 2005).

Sayers, C.M., 1994, The elastic anisotropy of shales: Journal of Geophysical Research, v. 99, p. 767-774, doi: 10.1029/93JB02579.

Silver, P.G., and Chan, W.W., 1991, Shear wave splitting and subcontinental mantle deformation: Journal of Geophysical Research, v. 96, p. 16,429-16,454.

Townend, J., and Zoback, M.D., 2001, Implications of earthquake focal mechanisms for the frictional strength of the San Andreas fault system, in Holdsworth, R.E., et al., eds., The nature and significance of fault zone weakening: Geological Society [London] Special Publication 186, p. 13-21.

Townend, J., and Zoback, M.D., 2004, Regional tectonic stress near the San Andreas fault in central and Southern California: Geophysical Research Letters, v. 31, p. L15S11.

Zhang, Z., and Schwartz, S.Y., 1994, Seismic anisotropy in the shallow crust of the Loma Prieta segment of the San Andreas fault system: Journal of Geophysical Research, v. 99, p. 9651-9661, doi: 10.1029/94JB00241.

Zinke, J.C., and Zoback, M.D., 2000, Structure-related and stress-induced shear wave velocity anisotropy: Observations from microearthquakes near the Calaveras fault in central California: Seismological Society of America Bulletin, v. 90, p. 1305-1312, doi: 10.1785/0119990099.

Zoback, M.D., and Zoback, M.L., 1991, Tectonic stress field of North America and relative plate motions, in Slemmons, D.B., et al., eds., Neotectonics of North America: Boulder, Colorado, Geological Society of America, Decade Map Volume 1, p. 339-366.

Zoback, M.D., Zoback, M.L., Mount, V.S., Suppe, J., Eaton, J.P., Healy, J.H., Oppenheimer, D., Reasenber, P., Jones, L., Raleigh, C.B., Wong, I.G., Scotti, O., and Wentworth, C., 1987, New evidence on the state of stress of the San Andreas fault system: Science, v. 238, p. 1105-1111.

Zoback, M.L., 1992, First and second order patterns of tectonic stress: The world stress map project: Journal of Geophysical Research, v. 97, p. 11,703-11,728.

Zoback, M.L., and Zoback, M.D., 1980, State of stress in the conterminous United States: Journal of Geophysical Research, v. 85, p. 6113-6156.

Zoback, M.L., Zoback, M.D., Adams, J., Assumpcao, M., Bell, S., Bergman, E.A., Bluemling, P., Denham, D., Ding, J., Fuchs, K., Gregersen, S., Gupta, H.K., Jacob, K., Knoll, P., Magee, M., Mercier, J.L., Muller, B.C., Paquin, C., Stephansson, O., Udias, A., and Xu, Z.H., 1989, Global patterns of intraplate stress: A status report on the world stress map project of the International Lithosphere Program: Nature, v. 341, p. 291-298, doi: 10.1038/341291a0.

Manuscript received 21 October 2005

Revised manuscript received 17 March 2006

Manuscript accepted 5 May 2006

Printed in USA